Phonon excitations and related thermal properties of aluminum nitride

J. C. Nipko and C.-K. Loong
Intense Pulsed Neutron Source Division, Argonne National Laboratory, Argonne, Illinois 60439-4814
(Received 9 January 1998)

The phonon density of states of aluminum nitride was determined by time-of-flight neutron spectroscopy using a polycrystalline sample. The observed phonon excitation spectrum consists of a broadband centered at about 35 meV, a small gap in the 75–80 meV region, and two sharp bands at approximately 85 and 92 meV. A rigid-ion model was applied to the interpretation of the data. After optimization, the model provided a satisfactory description of the neutron results as well as the Raman and IR data, sound-velocity measurements, and the lattice specific heat reported in the literature. The partial and total DOS and the phonon-dispersion curves along major symmetry directions of the Brillouin zone were calculated, and the contribution of phonons to the Debye behavior of the low-temperature thermal conductivity was discussed. [S0163-1829(98)00618-3]

I. INTRODUCTION

The unique properties of aluminum nitride have held high promise of advanced technological applications. It has a thermal conductivity comparable to most conductive metals (e.g., Al) and much greater than typical ceramics (about five times of that of alumina).[1] Its high electrical resistivity, good dielectric strength, thermal-expansion coefficient closely matching that of silicon, and lack of toxicity (unlike BeO) are ideal for microelectronic substrate applications.[2,3] Densified AlN has high strength (a flexural strength equivalent to alumina), high-temperature stability, and corrosion resistance.[4] Therefore, AlN ceramic components can potentially be used under extreme conditions.[2,5] Furthermore, AlN forms continuous alloy system with GaN and InN, exhibiting tunable band gaps which are suitable for optical devices operating at wavelengths over the red-to-ultraviolet region.[6,7]

Although AlN crystallizes in the hexagonal wurtzite structure which is the only stable phase at ambient pressure, the growth of single crystals has been difficult primarily due to the high melting temperature and the decomposition of the material at temperatures approaching the melting point.[8,9] Only small (maximum mm size) single crystals have been prepared thus far. A finely divided powder of AlN is relatively susceptible to hydrolysis, where AlN and water react to form aluminum hydroxide, ammonia, and heat.[10] Only until recently high-purity, pretreated water-resistant AlN powders have become available commercially.[2] In nonmetals such as AlN phonons are the primary excitations which influence the thermodynamic and transport properties. Although phonons can be investigated using several experimental techniques including Raman, infrared (IR), and neutron spectroscopy. Only neutrons can probe phonon modes throughout the Brillouin zone, and the method is not restricted by selection rules and is relatively insensitive to small amount of impurities. Like other diamondlike materials, the phonon frequencies of AlN are high (>100 meV). Perhaps for these reasons a measurement of the full phonon density-of-states (DOS) has not been reported in the literature, to our knowledge. The zone-center phonons obtained from Raman and IR measurements using small whisker crystals or films often do not favor a complete polarization analysis of the phonon mode symmetry,[11–17] although a full description of the five Raman-active phonons have been reported recently by McNeil, Grimsditch, and French.[18] No information regarding the phonon-dispersion relations is available. In this paper we report the determination of the phonon DOS of AlN obtained from time-of-flight neutron spectroscopy using a bulk powder. The satisfactory interpretation of the data by a lattice-dynamic model permits the calculation of the phonon-dispersion curves and the comparison of the lattice specific heat with previous experimental values.

II. EXPERIMENTAL DETAILS AND RESULTS

The neutron time-of-flight experiments were performed using the High-Resolution Medium-Energy Chopper Spectrometer (HRMECS) at the Intense Pulsed Neutron Source (IPNS) of Argonne National Laboratory. With a neutron incident energy (E_0) of 150 meV, the HRMECS spectrometer which is equipped with wide-angle multidetector banks allows measurements of inelastic scattering over a wide range of momentum ($\hbar\mathbf{Q}$) and energy (E) transfer: $4 \leqslant Q \leqslant 12$ Å^{-1}, $0 \leqslant E \leqslant 140$ meV. The summation of data over the wave vectors Q that are of much larger magnitudes than the crystal Brillouin-zone dimension is essential to the measurement of the phonon DOS under the incoherent approximation.[19–21] The energy resolution ΔE in full-width-at-half-maximum of the HRMECS spectrometer varies from approximately 4% of E_0 in the elastic region to $\sim 2\%$ near the end of the neutron-energy-loss spectrum.[22] The powder was contained in an aluminum planar cell mounted at a 45° angle to the incident neutron beam. Such a geometry decreases the neutron traverse length in the sample to <5 mm for all detector angles—thereby reducing multiple-scattering effects. To suppress as much as possible multiple-phonon excitations, the samples were cooled to 8 K for the experiments. Normal background scattering was subtracted from the data by using empty-container runs. Measurements of elastic incoherent scattering from a vanadium standard provided detector calibration and intensity normalization.

The AlN powders, acquired from Advanced Refractory Technology, Inc., were first characterized by conventional

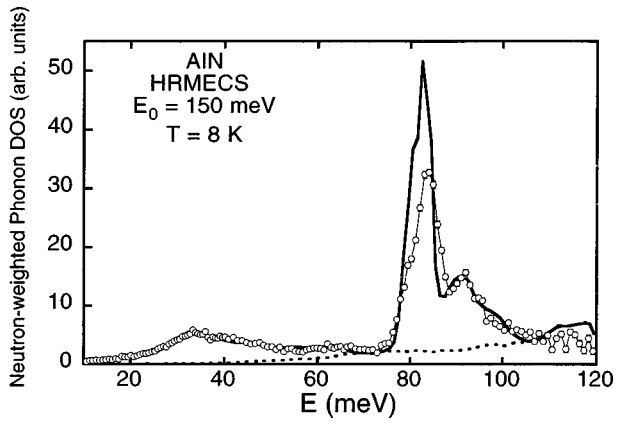

FIG. 1. Measured (open circles) and calculated (lines) neutron-weighted DOS for AlN. The solid line denotes the sum of the one-phonon and two-phonon DOS and the dashed line denotes the two-phonon contribution.

neutron powder diffraction using the General Purpose Powder Diffractometer also at IPNS. The material was found to consist of a single-phase wurtzite structure, space group $P6_3mc$ [at 297 K, $a=3.112$ Å, $c=4.980$ Å, atom positions at $(1/3,2/3,u)$ and $(1/3,2/3,u+1/2)$ with $u=0$ for Al and $u=0.382$ for N, Rietveld refinement weighted R factor$=6\%$], which is in good agreement with the previously reported structure.[4,23] The minimum average crystalline grain size was estimated to be ~ 1.5 μm. Since AlN powder is somewhat sensitive to moisture, the samples were stored in a dry nitrogen atmosphere or kept under vacuum during experiments.

The measured scattering function $S(Q,E)$ from a polycrystalline sample is effectively averaged over all crystallographic orientations. By summing the data over all observed Q values, a generalized phonon DOS can be obtained according to[24]

$$G(E)=\frac{2M}{\hbar^2}\left\langle \frac{e^{2W(Q)}}{Q^2}\frac{E}{n(E)+1}S(Q,E)\right\rangle$$

$$\approx M\sum_i \frac{c_i\sigma_i}{M_i}F_i(E), \qquad (1)$$

where c_i, σ_i, M_i, and $F_i(E)$ are the concentration, neutron-scattering cross section, the mass, and partial phonon DOS, respectively, for the ith atomic species (Al or N). M is a mean sample mass, $n(E)$ is the Bose-Einstein distribution function, and $\langle\cdots\rangle$ represents the average over all observed Q values. The Debye-Waller factor $e^{-2W(Q)}$ was estimated to be $e^{-0.003Q^2}$ in the present case based on the diffraction data. It can be seen from Eq. (1) that $G(E)$ provides a measure of the phonon DOS weighted by the $c_i\sigma_i/M_i$ factor, which is often referred to as the neutron-weighted phonon density of states.

The observed phonon spectrum (circles) of AlN at 8 K is shown in Fig. 1. It can be seen that the acoustic phonons extend up to about 30 meV, and the bands at about 35, 85, and 92 meV arise mainly from optical-phonon branches. The solid line represents the calculated neutron-weighted phonon spectrum based on a rigid-ion model (see the next section). There is a small gap in the DOS near the 70–75 region. The cutoff energy of the one-phone spectrum is about 105 meV. The two-phonon contribution accounts for the slowly rising background with increasing energies, filling the gap and the region beyond the one-phonon cutoff. Higher-order multiple-phonon components are negligible because they appear mainly at much higher energies.

III. LATTICE-DYNAMICS CALCULATIONS

The lattice dynamics of the wurtzite structure has been studied by many authors.[25–29] The group-theoretical analysis of the phonon branches can be found in Refs. 26 and 30–33, although the group notations vary among different authors. The readers may refer to the work by Warren and Worlton[34,35] for the convention of symmetry labels as well as a computer listing of the irreducible representations of the phonon modes along symmetry directions. The two formula units in a primitive cell result in 12-phonon branches. The symmetry decomposition at the zone center Γ consists of $2A_1+2B_1+2E_1+2E_2$ modes. Among the optic phonons, six modes, $E_1+E_2^{(1)}+E_2^{(2)}+2A_1$, are Raman active, and four modes, E_1+2A_1 are IR active.

A discrepancy of the order of 10% exists among the reported Raman and IR data probably due to the variation of sample form and quality used by different researchers.[11–18] The observed LO-TO splitting of the E_1 modes from Raman and IR investigations is indicative of some ionic character of the system. For example, from IR reflectivity measurements of polycrystalline AlN films deposited on glassy carbon substrates, Akasaki and Hashimoto reported the dielectric constants of $\varepsilon_0=8.50$ and $\varepsilon_\infty=4.68$ for the split E_1 mode.[11] Therefore, the lattice-dynamical model for the phonons of AlN has to account for the macroscopic electric field characteristic of Coulomb interactions between the ionic charges as well as possible polarization of the outer electronic orbitals of the ions. These effects may be mimicked using the shell model where a point-mass core representing a nucleus and its core electrons is connected with harmonic forces to a massless spherical shell representing the polarizable outer electrons in additional to Coulomb interactions.[36] However, unless ample phonon data over the Brillouin zone are available, it is not possible to fully refine the shell model in terms of a large numbers of adjustable parameters. Even in the favorable cases, the results of least-squares fits seldom reproduce the dielectric constants or provide physical insights into the mechanism of electronic polarization or screening. A rigid-ion model, on the other hand, allows Coulomb interactions between the ions thereby providing to some extent the proper LO-TO splitting of the zone-center phonons. However, by ignoring electronic polarizability, effectively assuming $\varepsilon_\infty=1$, the number of adjustable parameters is greatly reduced. Given that large single crystals of AlN are unavailable for neutron inelastic-scattering measurements of phonon-dispersion curves, we resorted to the use of the rigid-ion model to interpret the phonon DOS and optical data.

Based on the structural data from the powder diffraction, a rigid-ion model using the Born–von Kármán-type axially symmetric forces was constructed for wurtzite AlN. Radial and tangential force constants for the nearest- (NN) and the next-nearest-neighbor (NNN) interactions of Al-Al, N-N, and Al-N bonds were applied. The degree of ionicity of AlN

TABLE I. The parameter set for the rigid-ion model. F and G are the axially symmetric force constants for the radial and tangential components, respectively.

Bond type	Bond length (Å)	$F(r)$ (10^3 dyn/cm^2)	$G(r)$ (10^3 dyn/cm^2)
Al-N	1.889	206.0	2.3
Al-N	1.903	194.0	5.0
Al-Al	3.070	25.0	−1.0
N-N	3.070	18.0	−4.0
Al-N	3.077	−11.5	9.0
Al-Al	3.110	8.5	0.0
N-N	3.110	8.5	2.0

has been investigated by x-ray diffraction[23,37] and by first-principles Hartree-Fock and electronic band calculations.[38,39] The effective charge in the units of e associated with an ion was found to be between 1 and 2. For simplicity we fixed the charges for Al and N ions to be $+e$ and $-e$, respectively. This scheme required a total of 14 parameters. The summation of the long-range Coulomb forces was performed using the Ewald method. The dynamic matrix at the Γ point was block diagonalized using matrices constructed by the projection-operation method. This permitted the refinement of both the neutron and optical data. The setup of the dynamic matrix, the solution of the eigenvalue problem, and the calculation of the phonon DOS were carried out using the computer program GENAX written by Reichardt.[40]

The goal of the model calculation is to provide a reasonable interpretation of the observed neutron-weighted phonon DOS, optical data, and some related thermodynamic properties. First, the Raman frequencies of McNeil, Grimsditch, and French[18] were fitted by the model to obtain values of an initial subset of force constants. The partial phonon DOS, $F_{\mathrm{Al}}(E)$, and $F_{\mathrm{N}}(E)$, were computed by a root-sampling method by which the frequency-distribution functions were summed over 10^6 mesh points within the Brillouin zone. The neutron-weighted one-phonon DOS $G(E)$ was calculated according to Eq. (1) and convoluted with the resolution function HRMECS, and the two-phonon contribution was obtained from a self-convolution of the $G(E)$. The sum of the one- and two-phonon contributions was then compared with the measured spectrum. These steps were iterated until a satisfactory agreement between the observed and calculated spectrum was reached. This method did not aim for a determination of a unique parameter set which represents the absolute minimum of residue (χ^2) in the parameter space.[41] Instead, we looked for an internal consistence within the following criteria: (i) a reasonable scale between the NN and NNN force constants; (ii) a qualitative agreement with the Raman and IR data as well as with the measured sound velocities;[42] and (iii) a good agreement with the Debye temperature estimated from thermodynamic properties and with the measured lattice specific heat over a wide range of temperatures. The final parameter set, which are given in Table I, produced the neutron-weighted phonon DOS shown in Fig. 1. The overall agreement with the above criteria is good. The model overestimated the intensities of the optical band near 85 meV (see Fig. 1), probably due to an inadequate description of the LO-TO splitting and dispersion which is a known deficiency of the rigid-ion model. A comparison of the model calculations with the optical and sound velocity data is given in Table II.

TABLE II. A comparison of optical data (Ref. 18) and sound velocities (Ref. 42) with model calculation for AlN.

Mode	Measured frequency (meV)	Model calculation (meV)
A_1 (LO)	110.7	98.2
A_1 (TO)	76.1	75.6
$B_1{}^2$		92.4
$B_1{}^1$		70.2
E_1 (LO)	113.6	104.7
E_1 (TO)	83.4	83.9
$E_2{}^2$	81.8	80.6
$E_2{}^1$	31.2	32.9
	Measured velocity (km/s)	Calculated velocity (km/s)
ν_L	10.1	10.7
ν_s	6.3	6.2

IV. DISCUSSION

The neutron time-of-flight measurement of the phonon excitation spectrum of AlN does not correspond to the true phonon DOS because the neutron intensity is scaled according to the scattering cross sections of the Al and N nuclei. The coherent scattering cross sections of Al and N are 1.495 and 11.01 b, respectively (1 b=100 fm^2). Therefore, the observed neutron spectrum was weighted more favorable to the phonon modes which involve large N vibrational amplitudes. This can be seen by comparing the observed neutron-weighted DOS (Fig. 1) with the calculated partial and total DOS convoluted with the HRMECS resolution function, as shown in Fig. 2. The phonon DOS below the gap arises mainly from Al vibrations whereas the portion above the gap arises mainly from N vibrations.

The calculated phonon-dispersion curves along the major symmetry directions of the reduced Brillouin zone are plot-

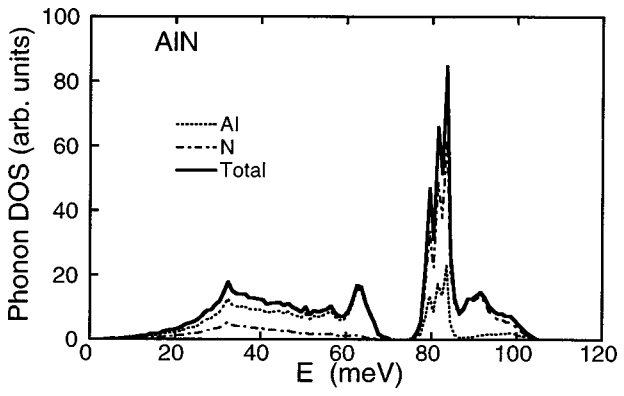

FIG. 2. The partial and total phonon DOS of AlN calculated from the rigid-ion model.

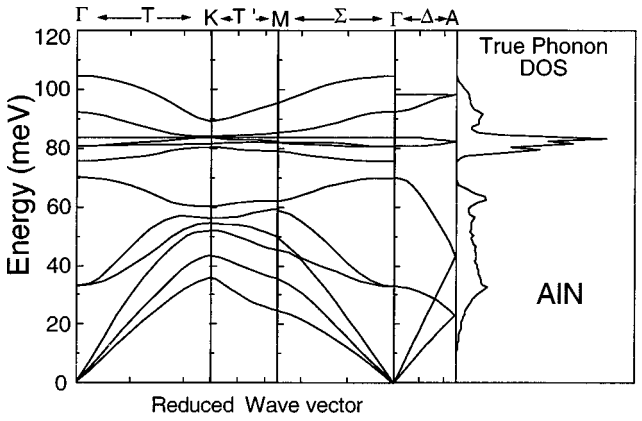

FIG. 3. The calculated phonon-dispersion curves of AIN along the major symmetry directions: $\Delta[0,0,x]$, $\Sigma[x,0,0]$, $T[x,x,0]$. The right panel: the true phonon DOS of AIN.

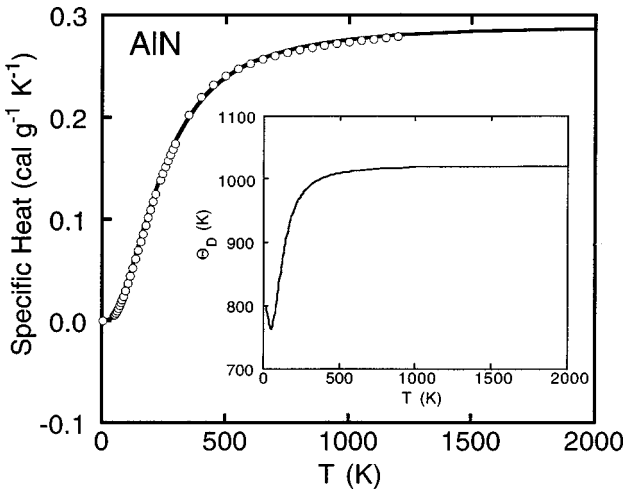

FIG. 4. The calculated (line) and measured (open circles) lattice specific heat for AIN (see text). The inset: the calculated temperature dependence of the Debye temperature.

ted in Fig. 3 together with the true DOS. The two sharp bands at about 85 and 92 meV arise from the six uppermost optic modes which exhibit little dispersion. A narrow gap separates these flat modes from the lower, more dispersive branches. The broad peak centered at ~ 35 meV contains many unresolved critical frequencies at the zone center and boundaries (van Hove singularities). Below ~ 30 meV the DOS exhibits the Debye-like $\sim E^2$ dependence. The steep longitudinal- and transverse-acoustic branches, and the high phonon cutoff frequency are consistent with the high hardness and mechanical strength of the material.

The lattice specific heat of AlN at constant volume C_v of AlN was evaluated using the phonon DOS predicted by the rigid-ion model. Figure 4 shows the calculated C_v and a comparison with the measured specific heat at constant pressure C_p reported by Koshchenko, Grinberg, and Demidenko.[43] The dilatation term, $C_p - C_v$, at 1200 K is estimated to amount to $\sim 1\%$ corrections. The agreement is very good over the entire measured temperature range up to about 1200 K. The calculated Debye temperature Θ_D as a function of temperature is shown in the inset of Fig. 4. The obtained Θ_D at 0 K of 800 K is in excellent agreement with those (800–825 K) estimated from specific-heat data.[7,43]

AlN belongs to a class of diamondlike (adamantine) compounds of which the thermodynamic properties such as thermal conductivity and thermal expansion are important factors relevant to the design of high-performance electronic packaging. For substrate application, high thermal conductivity and low thermal expansion are desirable. In the adamantine compounds each atom is coordinated by four nearest neighbors forming a tetrahedron. It is of interest to compare the thermal conductivity and the corresponding phonon DOS of these materials. We discuss only the qualitative features because the absolute conductivity depends critically on the microstructure and impurity level of the material.[44–46] At low temperatures the major limitation of heat conduction by phonons is scattering by external boundaries (e.g., domain size of a powder or sample dimensions of a single crystal). This gives rise to a $\sim T^3$ behavior of the thermal conductivity at low temperatures. In a typical log-log plot the thermal conductivity increases linearly, reaching a maximum at a characteristic temperature T_0, and then decreases with increasing temperature as phonon-phonon and phonon-defect scattering become the dominant processes. Diamond has the highest thermal conductivity and hardness. The phonon DOS of diamond exhibits a Debye-like region extending to ~ 65 meV and a cutoff energy of ~ 165 meV.[47,48] This results in a $\Theta_D(0\,\mathrm{K})$ exceeding 2000 K and a maximum in the thermal conductivity at $T_0 \cong 100$ K.[49,50] SiC has a Debye-like phonon DOS up to ~ 40 meV and a cutoff phonon-energy at ~ 130 meV.[51] The corresponding $\Theta_D(0\,\mathrm{K})$ and T_0 are 1185 and ~ 50 K, respectively.[49] Diamond and SiC are generally regarded as covalent bonded substances. BeO is another wurtzite compound of high ionicity, and it has been considered as a substrate material despite its toxicity. Its phonon DOS shows a Debye-like region up to ~ 40 meV and a cutoff energy of ~ 105 meV, and its $\Theta_D(0\,\mathrm{K})$ and T_0 are 1280 and ~ 45 K, respectively.[52–54]

By contrast, the phonon DOS of CdS, which is a semiconductor best known for its photoconduction of electricity, has a much different phonon DOS: a Debye-like region less than 6 meV and a cutoff energy of only 40 meV. It has a $\Theta_D(0\,\mathrm{K})$ of 210 K and a T_0 of ~ 10 K.[27,55,56] AlN has a phonon DOS similar to those of BeO and SiC, and its thermal conductivity peaks at $T_0 \cong 45$ K.[1] Therefore, aluminum nitride possesses the microscopic and macroscopic properties that are desirable for wide-bandgap semiconducting devices capable of operating at elevated temperatures.

In summary, we have measured the phonon DOS of an AlN powder by time-of-flight neutron spectroscopy. A rigid-ion model was applied to the interpretation of the lattice-dynamical and thermodynamic data. After optimization, a set of parameters was obtained which permitted a quantitative understanding of the phonon excitation spectrum, the optical data, and the lattice specific heat over a wide range of temperatures.

ACKNOWLEDGMENTS

Work performed at Argonne National Laboratory is supported by the U.S. DOE-BES under Contract No. W-31-109-ENG-38. We are grateful to W. Reichardt for providing the GENAX computer program for the lattice-dynamical calculations.

[1] G. A. Slack, R. A. Tanzilli, R. O. Pohl, and J. W. Vandersande, J. Phys. Chem. Solids **48**, 641 (1987).
[2] P. T. B. Shaffer and T. J. Mroz, *Aluminum Nitride* (Advanced Refractory Technology, Inc., 1991).
[3] F. E. Anderson, in *The Encyclopedia of Advanced Materials*, edited by D. Bloor, M. C. Flemings, R. J. Brook, and S. Mahajan (Pergamon, Oxford, 1994), Vol. 4, p. 2698.
[4] W. J. Meng, in *Properties of Group III Nitrides*, edited by J. H. Edgar (The Institution of Electrical Engineers, London, 1994), p. 22.
[5] D. D. Marchant and T. E. Nemecek, Adv. Ceram. **26**, 19 (1987).
[6] S. Strite and H. Morkoç, J. Vac. Sci. Technol. B **10**, 1237 (1992).
[7] J. H. Edgar, J. Mater. Res. **7**, 235 (1992).
[8] G. A. Slack and T. F. McNelly, J. Cryst. Growth **34**, 263 (1976).
[9] G. A. Slack and T. F. McNelly, J. Cryst. Growth **42**, 560 (1977).
[10] P. Bowen, J. Am. Ceram. Soc. **73**, 724 (1990).
[11] I. Akasaki and M. Hashimoto, Solid State Commun. **5**, 851 (1967).
[12] O. Brafman, G. Lengyel, S. S. Mitra, P. J. Gielisse, J. N. Plendl, and L. C. Mansur, Solid State Commun. **6**, 523 (1968).
[13] A. T. Collins, E. C. Lightowlers, and P. J. Dean, Phys. Rev. **158**, 833 (1967).
[14] C. Carlone, K. M. Lakin, and H. R. Shanks, J. Appl. Phys. **55**, 4010 (1984).
[15] P. Perlin, A. Polian, and T. Suski, Phys. Rev. B **47**, 2874 (1993).
[16] J. A. Sanjurjo, E. López-Cruz, P. Vogl, and M. Cardona, Phys. Rev. B **28**, 4579 (1983).
[17] K. Hayashi, K. Itoh, N. Sawaki, and I. Akasaki, Solid State Commun. **77**, 115 (1991).
[18] L. E. McNeil, M. Grimsditch, and R. H. French, J. Am. Ceram. Soc. **76**, 1132 (1993).
[19] V. S. Oskotskii, Sov. Phys. Solid State **9**, 420 (1967).
[20] M. M. Bredov, B. A. Kotov, N. M. Okuneva, V. S. Oskotskii, and A. L. Shakh-Budagov, Sov. Phys. Solid State **9**, 214 (1967).
[21] F. W. de Wette and A. Rahman, Phys. Rev. **176**, 784 (1968).
[22] C.-K. Loong, S. Ikeda, and J. M. Carpenter, Nucl. Instrum. Methods Phys. Res. A **260**, 381 (1987).
[23] H. Schulz and K. H. Thiemann, Solid State Commun. **23**, 815 (1977).
[24] D. L. Price and K. Sköld, in *Neutron Scattering*, edited by K. Sköld and D. L. Price (Academic, Orlando, 1986), Vol. A, p. 29.
[25] M. Tsuboi, J. Chem. Phys. **40**, 1326 (1964).
[26] M. A. Nusimovici and J. L. Birman, Phys. Rev. **156**, 925 (1967).
[27] M. A. Nusimovici and J. L. Birman, Phys. Rev. B **1**, 595 (1970).
[28] J. J. Sullivan, J. Phys. Chem. Solids **25**, 1039 (1964).
[29] V. L. Merten, Z. Naturforsch. A **15**, 512 (1960); **15**, 626 (1960); **17**, 65 (1960).
[30] R. C. Casella, Phys. Rev. **114**, 1514 (1959).
[31] M. L. Glasser, J. Phys. Chem. Solids **10**, 229 (1959).
[32] É. I. Rashba, Sov. Phys. Solid State **1**, 368 (1959).
[33] M. Nusimovici, J. Phys. (Paris) **26**, 689 (1965).
[34] J. L. Warren and T. G. Worlton, Comput. Phys. Commun. **3**, 88 (1972).
[35] J. L. Warren and T. G. Worlton, *Symmetry Properties of the Lattice Dynamics of Twenty-Three Crystals* (Argonne National Laboratory, 1973), Report No. ANL-8053 and LA-5465-MS (unpublished).
[36] K. Kunc and H. Bilz, in *Neutron Scattering*, edited by R. M. Moon (Oak Ridge National Laboratory, Gatlinburg, TN, 1976), Vol. I, p. 195.
[37] E. Gabe, Y. L. Page, and S. L. Mair, Phys. Rev. B **24**, 5634 (1981).
[38] E. Ruiz, S. Alvarez, and R. Alemany, Phys. Rev. B **49**, 7115 (1994).
[39] W. Y. Ching and B. N. Harmon, Phys. Rev. B **34**, 5305 (1986).
[40] W. Reichardt (private communication). The GENAX program also provides the options of using the shell and valence-force models.
[41] A procedure for least-squares fits of the observed DOS in terms of the model was also applied, but the fits did not produce a parameter set with smaller uncertainties.
[42] D. Gerlich, S. L. Dole, and G. A. Slack, J. Phys. Chem. Solids **47**, 437 (1986).
[43] V. I. Koshchendo, Y. K. Grinberg, and A. F. Demidenko, Inorg. Mater. **20**, 1550 (1985).
[44] G. A. Slack and S. F. Bartram, J. Appl. Phys. **46**, 89 (1975).
[45] G. A. Slack, *Solid State Physics: Advances in Research and Applications* edited by F. Seitz, D. Turnbull, and H. Ehrenreich (Academic, New York, 1979), Vol. 1, p. 1.
[46] W.-J. Kim, D. K. Kim, and C. H. Kim, J. Am. Ceram. Soc. **79**, 1066 (1996).
[47] R. Wehner, H. Borik, W. Kress, A. Goodwin, and S. D. Smith, Solid State Commun. **5**, 307 (1967).
[48] A. K. Ramdas, in *Properties and Growth of Diamond*, edited by G. Davies (INSPEC, London, 1994), p. 13.
[49] G. A. Slack, J. Phys. Chem. Solids **34**, 321 (1973).
[50] J. W. Vandersande, in *Properties and Growth of Diamond* (Ref. 48), p. 33.
[51] C.-K. Loong (unpublished).
[52] R. N. Sinclair, in *Inelastic Scattering of Neutrons in Solids and Liquids* (IAEA, Vienna, 1964), Vol. II, p. 199.
[53] R. M. Brugger, K. A. Strong, and J. M. Carpenter, J. Phys. Chem. Solids **28**, 249 (1967).
[54] G. A. Slack and S. B. Austerman, J. Appl. Phys. **42**, 4713 (1971).
[55] K. W. Böer, in *The Encyclopedia of Advanced Materials*, edited by D. Bloor, M. C. Flemings, R. J. Brook, and S. Mahajan (Pergamon, Oxford, 1994), Vol. 1, p. 301.
[56] E. F. Steigmeier, in *Thermal Conductivity*, edited by R. P. Tye (Academic, New York, 1969), Vol. 1, p. 203.